PAPER

MnO₂ aerogels for highly efficient oxidative degradation of Rhodamine B†

Hang Sun, [iD]* Yinxing Shang, Kongliang Xu, Yanan Tang, Jiayi Li and Zhenning Liu*

High-efficiency oxidative degradation of Rhodamine B (RhB) is demonstrated with manganese dioxide (MnO_2) aerogels. The MnO_2 aerogels are fabricated by an ice-templating approach from MnO_2 nanosheet colloids, which have been synthesized by redox reaction between $MnCl_2$ and $KMnO_4$ in sodium dodecyl sulfate (SDS) aqueous solution. The obtained self-standing MnO_2 aerogels show a three dimensional (3D) structure of a percolating network with open pores ranging from hundreds of nanometers to tens of micrometers. The oxidative degradation efficiency of MnO_2 aerogels is compared with ultrathin MnO_2 nanosheets and commercial MnO_2 powder, and the effects of concentration of MnO_2 aerogels as well as pH on the degradation efficiency are also investigated. Typically, the MnO_2 aerogels show an excellent oxidative degradation performance of RhB (97.6% removed within 10 min) in acidic solution (pH 2.5), which can be attributed to the large open pores and high surface areas of the aerogels. Furthermore, the MnO_2 aerogels also exhibit good capability in the degradation of methylene blue (MB) under acidic conditions. It is believed that MnO_2 aerogels hold great promise for future applications in organic pollutant removal with virtues of high efficiency, low cost and environmental friendliness.

Introduction

The environmental contamination caused by organic pollutants has become a serious global problem with economic development and population growth. Organic dyes, often used in food and textile industries, are major sources of environmental contamination due to their high toxicity to aquatic creatures and carcinogenic effects on human beings.[1–3] Applications of conventional physical and biological methods for the treatment of organic dyes in surface and ground water are limited by a series of factors, including high cost, tedious processes,[4] demanding conditions and long degradation time, *etc.* Recently, some novel techniques have been developed to decontaminate surface and ground water, such as semiconductor photocatalysis and active metal oxide oxidation.[5–8] Nevertheless, it still remains a grand challenge to further elevate oxidative degradation efficiency.

Manganese dioxide (MnO_2) has been increasingly utilized in oxidative degradation due to its variable valence, abundance, low cost, non-toxicity and little secondary pollution. In particular, MnO_2 nanostructures of high specific surface area have been known of superior property in the degradation of organic pollutants. Jinbo Fei and co-workers have demonstrated

a controlled preparation of hierarchical hollow MnO_2 nanostructures and their application in efficient oxidative degradation of Congo red.[9] Yu Xin Zhang and co-workers have shown a pH-dependent degradation of methylene blue (MB) by the birnessite-type MnO_2 nanosheets on fiberglass.[10] Huihua Peng and co-workers have reported MnO_2 nanostructures of two different crystalline (*i.e.* α-MnO_2 and δ-MnO_2), which can be uniformly deposited on diatomite to absorb and degrade methyl orange. It is found the δ-MnO_2 nanosheets incur a faster reaction rate.[11] Recently, aerogels typically with macroscopic sponge-like three dimensional (3D) architectures have exhibited good performance in capacitors, lithium ion battery, catalysis, toxicant absorption, *etc.* We have envisioned that MnO_2 aerogels assembled by MnO_2 nanosheets, which have larger surface area and better crystalline than MnO_2 powders, hold great promise to improve the oxidative degradation of organics, owing to their low density, large open pores and high surface area. However, there is no relevant report yet.

Herein, we have developed a simple one-step approach to synthesize ultrathin MnO_2 nanosheets *via* the redox reaction between $MnCl_2$ and $KMnO_4$ in the presence of sodium dodecyl sulphate (SDS). Then self-standing MnO_2 aerogels have been prepared by freeze-drying the resultant nanosheet colloid and used in the degradation of RhB directly. We have compared the oxidative degradation efficiency of Rhodamine B (RhB) by the obtained MnO_2 aerogels with those of ultrathin MnO_2 nanosheets and commercial MnO_2 powder, and further investigated the effects of concentration of MnO_2 aerogel as well as pH on

Key Laboratory of Bionic Engineering (Ministry of Education), College of Biological and Agricultural Engineering, Jilin University, Changchun, Jilin Province, 130022, China. E-mail: sunhang@jlu.edu.cn; liu_zhenning@jlu.edu.cn

the degradation efficiency. In addition, we have tested the degradation of MB by MnO_2 aerogels. The mechanism for the highly efficient oxidative degradation of organic dyes by MnO_2 aerogels is also discussed.

Experimental

Materials

$KMnO_4$ (A.R.), ethanol (A.R.) and concentrated sulfuric acid (H_2SO_4, A.R.) were obtained from Beijing Chemical Works. $MnCl_2$ (C.P.) was obtained from Tianjin Fuchen Chemical Reagents Factory. Sodium dodecyl sulphate (SDS, C.P.) and Rhodamine B (RhB, A.R.) were purchased from Tianjin Guangfu Fine Chemical Research Institute. Commercial MnO_2 (A.R.) was purchased from Tianjin Huadong Chemical Reagent Works. All chemicals were used without any purification. Deionized water (resistance > 18 MΩ cm^{-1}) was used throughout this study.

Synthesis of MnO_2 colloid

MnO_2 colloids were synthesized through a redox reaction between $KMnO_4$ and $MnCl_2$ in the presence of SDS. First, SDS aqueous solution (10 mM, 297 mL) was heated at 100 °C for 15 min. $MnCl_2$ solution (50 mM, 1.8 mL) was then added dropwise into the above solution followed by the quick injection of $KMnO_4$ solution (50 mM, 1.2 mL) under rapid stirring to start the reaction. The total volume of the solution was 300 mL, where [SDS] = 10 mM, [Mn^{2+}] = 0.3 mM, [MnO_4^-] = 0.2 mM. After the resultant mixture was continued heating for 3 hours, the solution became colorless and the ultrathin MnO_2 nanosheets formed had been precipitated. Then the precipitates were washed repeatedly with ultrapure water and alcohol for purification. At last, the purified MnO_2 precipitates were redispersed in 10 mL of water and sonicated to yield homogeneous MnO_2 nanosheet colloids.

Fabrication of MnO_2 aerogel

MnO_2 aerogels were fabricated by an ice-templating approach from ultrathin MnO_2 nanosheet colloid. First, the ultrathin MnO_2 nanosheet colloid (1.35 g L^{-1}) was frozen at −20 °C for 12 hours to form brown ice-containing chunk.[12] Then a freeze dryer was used to remove the ice in the ice-containing chunk by sublimation to get a self-standing MnO_2 aerogel without observable structure collapse or volume shrinkage.

Material characterization

Transmission electron microscopy (TEM) images were obtained with a JEOL-2010 electron microscope operating at 200 kV. Atomic force microscopy (AFM) under tapping mode was carried out with a commercial instrument (Digital Instrument, Nanoscope III, and Dimension 3000) at room temperature in air. Scanning electron microscopy (SEM) images were collected on a JEOL JSM-7500F field emission scanning electron microscope (FE-SEM). X-ray diffraction (XRD) was performed on a SHIMADZU X-ray diffractometer (D/max rA, using Cu Kα radiation was at a wavelength of 1.542 Å), and the data were collected from 5° to 80°. X-ray photoelectron spectroscopy (XPS)

analysis was performed using a Kratos-Axis spectrometer with monochromatic Al Kα (1486.71 eV) X-ray radiation (15 Kv and 10 mA) and hemispherical electron energy analyzer. Total organic carbon (TOC) investigation was examined in Vario TOC cube (Elementar, Germany).

Oxidative degradation of RhB

The RhB aqueous solution with the concentration of 5 mg L^{-1} was prepared, the pH value of which is 5.9. The RhB aqueous solutions with different pH values of 2.5 and 3.5 were obtained by adjusting with H_2SO_4 solution (0.1 M). Then quantitative MnO_2 aerogel was added into 10 mL RhB solution under dark condition at room temperature with magnetic stirring. At given time intervals, the mixed solution of 0.8 mL was pumped by a disposable syringe and filtrated quickly (filter head pore size: 0.22 micron) to remove MnO_2 aerogel to quench the reaction. Then, the filtrates were analyzed, using a SHIMADZU UV-2550 UV-vis spectrophotometer, by recording the variations in the absorption band in the UV-visible spectra of RhB. Oxidative degradation of RhB by ultrathin MnO_2 nanosheets which were obtained by drying ultrathin MnO_2 nanosheet precipitate at 90 °C as well as commercial MnO_2 powder were also examined.

Result and discussion

Characterization of MnO_2 nanosheets

A representative transmission electron microscopy (TEM) image of the synthesized MnO_2 nanosheets is shown in Fig. 1a, in which transparent lamellar structure with abundant graphene-like wrinkles and folds can be observed, displaying a typical 2 dimensional (2D) morphology of MnO_2 nanosheets.[13] The lateral dimension of the nanosheets is mainly in the range of 80 to 200 nm. The thickness of MnO_2 nanosheets is estimated as 1.14 nm as measured by AFM (Fig. S1†), in line with the reported thickness for a single layer of MnO_2 nanosheets.[14] The crystal structure of the as-prepared MnO_2 nanosheets has been examined by X-ray diffraction (XRD). As shown in Fig. 1b, the XRD profile exhibits diffraction peaks at $2\theta = 12.2°, 24.7°, 36.8°,$ and $66.0°$, which agree with the characteristic peaks of δ-MnO_2 (JCPDS no. 18-0802).[15] Notably, the lattice spacing (d) of the plane (001), corresponding to the prominent spike at $2\theta = 12.2°$, is 0.725 nm ($d_{001} = 0.725$ nm).[16,17] The peaks at $2\theta = 24.7°, 36.8°$ and $66.0°$, corresponding to d values of approximately 0.360, 0.244 and 0.141 nm, can be indexed to the (002), (100) and (110) planes of δ-MnO_2, respectively.[18]
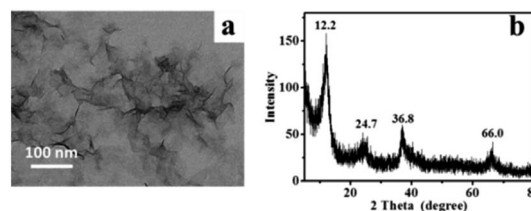

Fig. 1 (a) TEM image of the MnO_2 nanosheets; (b) XRD profile of the MnO_2 nanosheets.
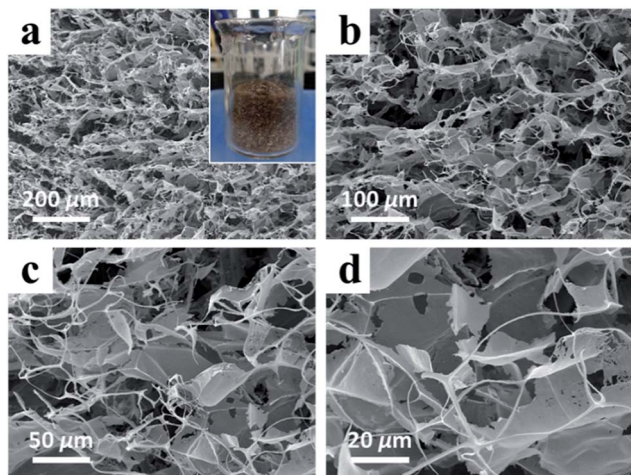
Fig. 2 (a–d) SEM images of the MnO$_2$ aerogels at the same observation location but of different magnifications, which increase from low (a) to high (d); inset of (a) is the photograph of the as-prepared MnO$_2$ aerogel.

Characterization of MnO$_2$ aerogels

High-purity MnO$_2$ aerogels were self-assembled from monodispersed MnO$_2$ nanosheets by fully manipulating the interactions between MnO$_2$ nanosheets *via* an ice-templating approach.[19] Specifically, the colloids of ultrathin MnO$_2$ nanosheets were first made by the ultrasound-exfoliation of purified layered MnO$_2$ nanosheets.[13,19] Subsequently, a 3D network was formed by cultivating a colloid of MnO$_2$ nanosheets at a temperature of −20 °C, which was confined by the growing ice crystals. A free-standing cylindrical MnO$_2$ aerogel (inset of Fig. 2a) can be prepared through the sublimation of ice in a freeze-dryer, which shows a biomimetic foam structure with interconnected macro-pores visible to naked eyes. In order to further characterize the micro-morphology of the obtained aerogels, scanning electron microscopy (SEM) has been employed, which revealed a 3D percolating network with open pores ranging from hundreds of nanometers to tens of micrometers (Fig. 2), confirming the successful self-assembly of 2D MnO$_2$ nanosheets into macroscopic structure. As the magnification increases from low (Fig. 2a) to high (Fig. 2d), it becomes evident that the 3D network is mainly constituted by 2D flakes and 1D rods. The average length of the 1D rods is estimated as ∼30 μm (Fig. S2†), whereas the 2D flakes show a lateral dimension of ∼50 μm. These 1D rods usually possess a prismatic shape with concaved sides, and three joined 1D rods form a "Y-shaped" trident node, which can be found ubiquitously in the SEM images.

X-ray photoelectron spectroscopy (XPS) was conducted to determine the chemical composition of the obtained aerogels (Fig. 3). Fig. 3a exhibits two peaks of Mn at 641.5 and 652.8 eV, which can be indexed to Mn$_{2p3/2}$ and Mn$_{2p1/2}$ of MnO$_2$, respectively.[16,20] No characteristic signal of Mn(II), Mn(III) and Mn(VII) has been identified in the XPS spectrum. The XPS spectrum for O$_{1s}$ is displayed in Fig. 3b, which shows two peaks at 528.5 and 531.8 eV, representing two species of oxygen in the
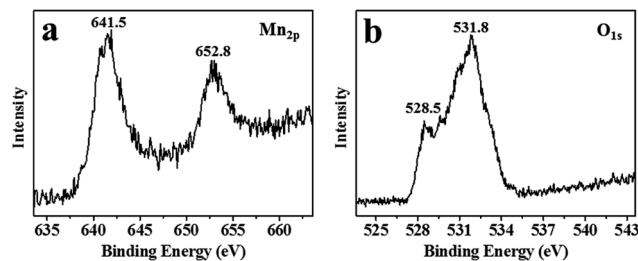

Fig. 3 XPS spectrum of the MnO$_2$ aerogels. (a) For Mn$_{2p}$: 641.5 and 652.8 eV correspond to Mn$_{2p3/2}$ and Mn$_{2p1/2}$ in MnO$_2$; (b) for O$_{1s}$: 528.5 and 531.8 eV correspond to O$_{1s}$ in the lattice of [MnO$_6$] octahedra and the interlayer H$_2$O or H$_3$O$^+$.

obtained MnO$_2$ aerogel: one in the lattice of [MnO$_6$] octahedra and the other in the interlayer H$_2$O or H$_3$O$^+$.[3]

Oxidative degradation of RhB

The oxidative degradation ability of the as-prepared MnO$_2$ aerogels was examined by the degradation of RhB, together with controls of grinded MnO$_2$ aerogel powder, MnO$_2$ nanosheets powder, commercial MnO$_2$ powder (Fig. 4). The grinded MnO$_2$ aerogel powder was used to see whether the characteristic feature of the aerogels could be damaged by the degradation reaction. As the degradation proceeded, the color of RhB solution quickly changed from pink to faint yellow and finally turned colorless within 10 min (Fig. 4a, inset). As shown in Fig. 4a, with the action of MnO$_2$ aerogel, the characteristic peak of RhB at the wavelength of 556 nm rapidly decreased accompanied with an evident blue shift from 556 to 498 nm. There are two possible pathways for the degradation of RhB. One is preceded by the generation of a carbon-centered radical with
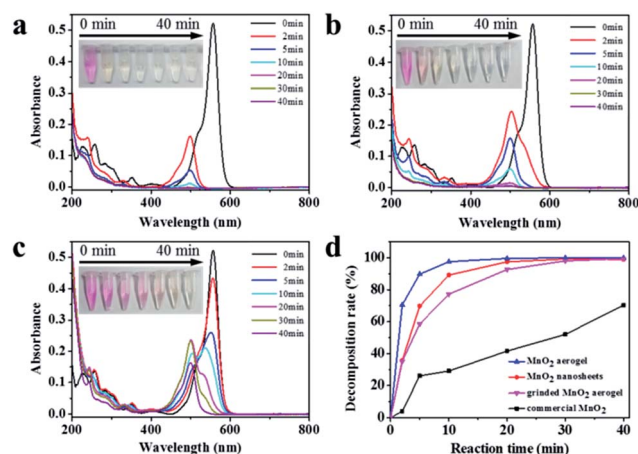

Fig. 4 UV-vis absorption spectra of RhB aqueous solution (5 mg L^{-1}, pH = 2.5) after different durations with different kinds of MnO$_2$ (0.5 g L^{-1}): (a) MnO$_2$ aerogel, (b) MnO$_2$ nanosheets powder, and (c) commercial MnO$_2$ powder, insets are the corresponding photographs of RhB aqueous solution during the degradation. (d) Plots of RhB degradation with different kinds of MnO$_2$: MnO$_2$ aerogel (blue triangle), grinded MnO$_2$ aerogel powder (pink inverted triangle), MnO$_2$ nanosheets powder (red circle), commercial MnO$_2$ powder (black square).

the breakdown of the aromatic ring directly. The other is *via* the formation of a nitrogen-centered radical, which undergoes a two-step reaction of *N*-deethylation and subsequent destruction of the backbone.[21–25] In our case, the blue shift of the characteristic peak to around 498 nm agrees with the *N*-deethylation process. Meanwhile, the decoloration of the solution and the decrease in the absorption peak indicate the destruction of the conjugated xanthene structure.[21,24,26,27] Therefore, the oxidative degradation of RhB by our MnO_2 aerogels is likely through the second pathway. Simultaneously, the MnO_2 aerogel was reduced from Mn(IV) to Mn(II) by RhB and its derivatives.[28]

The commercial MnO_2 powder and MnO_2 nanosheets powder of same concentration (0.5 g L^{-1}) were used in the decomposition of RhB for comparison. As seen in Fig. 4b, for MnO_2 nanosheets powder, the color change of RhB solution is slower than that of MnO_2 aerogels, suggesting an increased activity of MnO_2 nanosheets after self-assembling into the aerogel. In contrast, for the commercial MnO_2 powder (Fig. 4c), the pink color of RhB solution faded more slowly, and after 40 min, it still remained pale yellow. It should be noted that the characteristic peak of an intermediates of RhB degradation at the wavelength of 498 nm first rose and then fell (Fig. 4c), which is also in line with the second two-step mechanism as discussed above.

In order to evaluate the degradation ability of these materials quantitatively, the plots of RhB degradation with different kinds of MnO_2 were obtained by eqn (1),

$$D = \frac{A_0 - A}{A_0} \times 100\% \tag{1}$$

in which *D* represents the decomposition ratio of RhB at each designated time point during the reaction, and A_0 and A are the integrated area of the characteristic peak at 0 min and at each designated time point, respectively. At 40 min, the decomposition efficiency for MnO_2 aerogel, MnO_2 nanosheets powder and commercial MnO_2 powder are 100%, 99.0% and 70.3%, respectively. The high oxidative degradation efficiency of MnO_2 aerogel and MnO_2 nanosheets can be ascribed to their large active surface areas, which afford higher probability for Mn(IV) to be reduced to Mn(II) upon the contact with RhB. At 10 min, the oxidative degradation efficiency of MnO_2 aerogel and MnO_2 nanosheets powder are 97.6% and 89.2%, which are much faster than that of commercial MnO_2 powder (29.1%) (Fig. 4d). In the case of MnO_2 aerogels, 2D MnO_2 nanosheets are assembled into a 3D percolating network with open pores, which not only prohibits the aggregation of 2D MnO_2 nanosheets but also allows easier passage of RhB and its degradation products during the reaction, leading to enhanced oxidative degradation rate. When the MnO_2 aerogel was grinded into powder with agate mortar[29] and used for the decomposition of RhB, 99.5% of RhB was degraded within 40 min. Yet, the oxidative degradation efficiency at 10 min is only 77.2% (Fig. 4d). Thus, the 3D percolating network with open pores, as that in MnO_2 aerogels can indeed benefit degradation rate significantly.

As discussed above, RhB is mineralized stepwise *via* *N*-deethylation and backbone destruction, instead of decomposition to CO_2 directly. Hence, the loss of RhB absorption doesn't

necessarily mean the full degradation. To this end, total organic carbon (TOC) was measured to assess the level of organic removal. A TOC loss approximately of 92.1% was achieved after 40 min of oxidative degradation of RhB by MnO_2 aerogel (pH = 2.5). The observed smaller loss of TOC compared to the disappearance of UV-vis absorption is common in the oxidative degradation of organics by metal oxides, suggesting a multi-step degradation that takes longer time than the color change.[30,31]

Various concentrations of MnO_2 aerogels were then examined for the degradation of RhB to obtain the optimal concentration. As shown in Fig. 5a and b, the MnO_2 aerogels at the concentration of 1 g L^{-1} and 0.1 g L^{-1} resulted in similar blue shift and decrease of the characteristic RhB peak as those in the case of 0.5 g L^{-1}, and the RhB characteristic peak disappeared at 70 min, indicating the complete loss of RhB. Further comparison in plots of RhB degradation shows that the concentration of MnO_2 aerogel can indeed influence the degradation rates of RhB. As shown in Fig. 5c, when the MnO_2 aerogel concentration increases from 0.1 g L^{-1} to 0.5 g L^{-1}, the degradation ratio does increase from 54.6% to 97.6% at 10 min. However, a slight decrease of the oxidative rate to 86.8% was observed when the concentration of MnO_2 aerogel further increased to 1 g L^{-1}, which may be attributed to the aggregation of MnO_2 aerogel at an extremely high concentration. Therefore, we used the concentration of 0.5 g L^{-1} in further studies.[32] It is also noteworthy that the oxidation ability of our MnO_2 aerogels is superior to those of other MnO_2-based and H_2O_2-based materials (Table S1†).

It is known that in the degradation of RhB, the pH of the solution also plays an important role. Therefore, the effect of pH on the degradation efficiency was also examined (Fig. 5d–f). As shown in Fig. 5d, at pH 3.5, a slight decoloration of RhB solution can be observed in 5 min, but after 5 min the solution remains unchanged, suggesting that the oxidation capability of MnO_2 aerogels has been attenuated under the increased pH value. When the pure RhB dye (5 mg L^{-1} pH = 5.9) without the adjustment of pH value was tested (Fig. 5e), no evident discoloration and shift of the characteristic peak were observed with extending time. Therefore, it is conceivable that the fluctuations in the plots of RhB degradation at pH of 3.5 and 5.9 were caused by the adsorption removal of RhB molecules by MnO_2 aerogels (Fig. 5f), especially with the consideration of its 3D percolating network with open pores.

Obviously, low pH value can improve the decomposition efficiency of RhB. As a matter of fact, the redox reaction of δ-MnO_2/Mn^{2+} is expressed as δ-MnO_2(s) + 4H^+ + 2e^- → Mn^{2+}(aq) + 2H_2O, which has a standard reducing potential φ° equal to 1.29 V.[13] The reducing potential of δ-MnO_2/Mn^{2+} can be improved by low pH value, which means that low pH can facilitate the oxidation process.

Based on the literature, it is believed that Mn(IV) is reduced to Mn(II) in our case after the reaction, which remains soluble in the low pH solution.[33] It has been reported that MnO_2 can be converted to Mn(II) under low pH condition, generating strong oxidizing hydroxyl radicals ('OH).[34] These radicals can subsequently react with a dye or other organic compounds to yield a whole range of intermediates including radical and radical
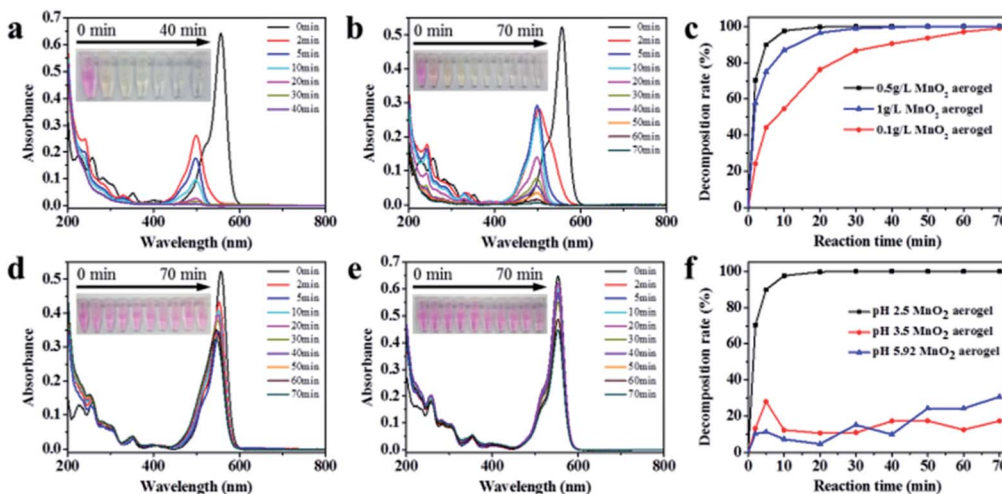
Fig. 5 (a–c) UV-vis absorption spectra of RhB aqueous solution (5 mg L^{-1}, pH = 2.5) after different durations with MnO$_2$ aerogels of different concentrations: (a) 1 g L^{-1}, (b) 0.1 g L^{-1}, and (c) plots of RhB degradation at pH = 2.5 with different MnO$_2$ aerogel concentrations: 0.1 g L^{-1} (red circle), 0.5 g L^{-1} (black square), 1 g L^{-1} (blue triangle). (d–f) UV-vis absorption spectra of RhB aqueous solution (5 mg L^{-1}) after different durations with MnO$_2$ aerogels at the same concentration of 0.5 g L^{-1} but different pH: (d) pH = 3.5, (e) pH = 5.9, and (f) plots of RhB degradation at different pH: pH = 2.5 (black square), pH = 3.5 (red circle), pH = 5.9 (blue triangle). Insets in (a and b) and (d and e) are the corresponding photographs of RhB aqueous solution during degradation.
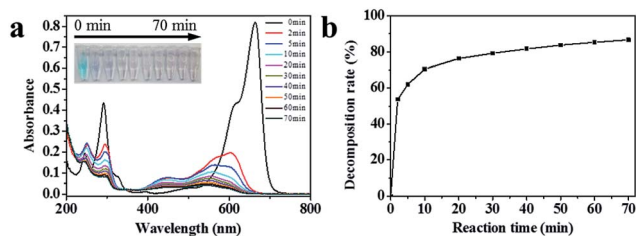
Fig. 6 (a) UV-vis absorption spectra of MB aqueous solution (5 mg L^{-1}, pH = 2.5) after different durations with MnO$_2$ aerogels. Inset is the corresponding photograph of MB aqueous solution during degradation. (b) Plot of MB degradation.

cations, leading to a complete mineralization with the formation of CO$_2$, H$_2$O, and NO$_3^-$.[35,36]

Furthermore, we have also studied the oxidative degradation of MB by our MnO$_2$ aerogels. The color of MB solution changed from blue to faint pink within 10 min, and the faint pink gradually faded with time (Fig. 6a, inset). The UV-vis absorption spectra of MB aqueous solution show three characteristic peaks at the wavelength of 249 nm,[37] 290 nm[38] and 663 nm,[39] respectively (Fig. 6a). According to previous reports,[40] the peak at 663 nm represents a blue shift because of the N-demethylation of MB, the intermediates of which cause the pink color. With the reaction continues, the peaks at 633 and 290 nm decrease simultaneously, implying that the backbone of MB has been destructed. The peak at 249 nm is ascribed to leuco-methylene blue (LMB), a secondary reduced product of MB, which is colorless and stable in MB aqueous solutions.[39] The oxidative decomposition of LMB leads to the loss of peak at 249 nm.

The plot of MB degradation is made by integrating the area under the characteristic peak at 663 nm. As illustrated in Fig. 6b, the decomposition surged up to 53.7% in 2 min, after

which the degradation efficiency declined gradually. At 70 min, 86.7% of MB was decomposed and the corresponding TOC removal was 59.5%. Together the excellent degradation of RhB and MB indicate that the MnO$_2$ aerogel holds great promise for future applications in organic pollutant removal.

Conclusions

In summary, high-efficiency oxidative degradation of RhB solution has been demonstrated for MnO$_2$ aerogels. The MnO$_2$ aerogels were prepared via a facile synthesis of MnO$_2$ nanosheets by redox reaction between MnCl$_2$ and KMnO$_4$ in the presence of SDS, followed by an ice-templating approach from MnO$_2$ nanosheet colloids. The MnO$_2$ aerogels possess 3D percolating network with open pores, which not only prohibits the aggregation of 2D MnO$_2$ nanosheets but also allows easier passage of RhB and its degradation products during the reaction, leading to enhanced oxidative degradation efficiency compared to those of the commercial MnO$_2$ powder and MnO$_2$ nanosheets. Moreover, the contribution from a favorable crystalline in the aerogels may also benefit the reaction. Typically, MnO$_2$ aerogels show a high and rapid oxidative degradation of RhB (97.5% removed within 10 min) in acid solution (pH 2.5). Furthermore, MnO$_2$ aerogels also exhibit good performance in the degradation of MB. It is believed that MnO$_2$ aerogel, as a high-efficiency, cost-effective and environment-friendly material, holds great promise for future applications in organic pollutant removal.

Acknowledgements

References

1 V. Eskizeybek, F. Sari, H. Gulce, A. Gulce and A. Avci, *Appl. Catal., B*, 2012, **119**, 197–206.

2 J. Kim, Y. Park and H. Park, *Int. J. Photoenergy*, 2014, **2014**, 324859.

3 C. A. Martinez-Huitle and E. Brillas, *Appl. Catal., B*, 2009, **87**, 105–145.

4 M. M. El-Sheekh, M. M. Gharieb and G. W. Abou-El-Souod, *Int. Biodeterior. Biodegrad.*, 2009, **63**, 699–704.

5 Y. Xu, Y. Huang and B. Zhang, *Inorg. Chem. Front.*, 2016, **3**, 591–615.

6 A. J. Cowan, W. H. Leng, P. R. F. Barnes, D. R. Klug and J. R. Durrant, *Phys. Chem. Chem. Phys.*, 2013, **15**, 8772–8778.

7 M. K. Kumar, S. Krishnamoorthy, L. K. Tan, S. Y. Chiam, S. Tripathy and H. Gao, *ACS Catal.*, 2011, **1**, 300–308.

8 X. J. Lang, J. C. Zhao and X. D. Chen, *Angew. Chem., Int. Ed.*, 2016, **55**, 4697–4700.

9 J. B. Fei, Y. Cui, X. H. Yan, W. Qi, Y. Yang, K. W. Wang, Q. He and J. B. Li, *Adv. Mater.*, 2008, **20**, 452–456.

10 Y. X. Zhang, X. L. Guo, M. Huang, X. D. Hao, Y. Yuan and C. Hua, *J. Phys. Chem. Solids*, 2015, **83**, 40–46.

11 H. H. Peng, J. Chen, D. Y. Jiang, M. Li, L. Feng, D. Losic, F. Dong and Y. X. Zhang, *J. Colloid Interface Sci.*, 2016, **484**, 1–9.

12 K. Xu, X. Zhu, P. She, Y. Shang, H. Sun and Z. Liu, *Inorg. Chem. Front.*, 2016, **3**, 1043–1047.

13 H. Sun, K. Xu, M. Huang, Y. Shang, P. She, S. Yin and Z. Liu, *Appl. Surf. Sci.*, 2015, **357**, 69–73.

14 Z. N. Liu, K. L. Xu, H. Sun and S. Y. Yin, *Small*, 2015, **11**, 2182–2191.

15 S. Devaraj and N. Munichandraiah, *J. Phys. Chem. C*, 2008, **112**, 4406–4417.

16 G. X. Zhao, J. X. Li, L. Jiang, H. L. Dong, X. K. Wang and W. P. Hu, *Chem. Sci.*, 2012, **3**, 433–437.

17 A. K. Sinha, M. Pradhan and T. Pal, *J. Phys. Chem. C*, 2013, **117**, 23976–23986.

18 S. Chen, J. W. Zhu, Q. F. Han, Z. J. Zheng, Y. Yang and X. Wang, *Cryst. Growth Des.*, 2009, **9**, 4356–4361.

19 Z. Liu, K. Xu, P. She, S. Yin, X. Zhu and H. Sun, *Chem. Sci.*, 2016, **7**, 1926–1932.

20 L. L. Peng, X. Peng, B. R. Liu, C. Z. Wu, Y. Xie and G. H. Yu, *Nano Lett.*, 2013, **13**, 2151–2157.

21 K. Yu, S. G. Yang, H. He, C. Sun, C. G. Gu and Y. M. Ju, *J. Phys. Chem. A*, 2009, **113**, 10024–10032.

22 G. M. Liu, X. Z. Li, J. C. Zhao, H. Hidaka and N. Serpone, *Environ. Sci. Technol.*, 2000, **34**, 3982–3990.

23 S. Horikoshi, A. Saitou, H. Hidaka and N. Serpone, *Environ. Sci. Technol.*, 2003, **37**, 5813–5822.

24 T. Watanabe, T. Takizawa and K. Honda, *J. Phys. Chem.*, 1977, **81**, 1845–1851.

25 D. Zhang, J. Li, Q. G. Wang and Q. S. Wu, *J. Mater. Chem. A*, 2013, **1**, 8622–8629.

26 Y. M. Xie, L. Lv, S. J. Zhang, B. C. Pan, X. S. Wang, Q. Chen, W. M. Zhang and Q. X. Zhang, *Nanotechnology*, 2011, **22**, 305707.

27 H. B. Fu, S. C. Zhang, T. G. Xu, Y. F. Zhu and J. M. Chen, *Environ. Sci. Technol.*, 2008, **42**, 2085–2091.

28 G. X. Zhao, J. X. Li, X. M. Ren, J. Hu, W. P. Hu and X. K. Wang, *RSC Adv.*, 2013, **3**, 12909–12914.

29 D. Y. Qi, L. J. Lu, L. Z. Wang and J. L. Zhang, *J. Am. Chem. Soc.*, 2014, **136**, 9886–9889.

30 H. B. Fu, C. S. Pan, W. Q. Yao and Y. F. Zhu, *J. Phys. Chem. B*, 2005, **109**, 22432–22439.

31 S. Horikoshi, H. Hidaka and N. Serpone, *Environ. Sci. Technol.*, 2002, **36**, 1357–1366.

32 Y. X. Zhang, X. D. Hao, F. Li, Z. P. Diao, Z. Y. Guo and J. Li, *Ind. Eng. Chem. Res.*, 2014, **53**, 6966–6977.

33 T. Takashima, K. Hashimoto and R. Nakamura, *J. Am. Chem. Soc.*, 2012, **134**, 18153–18156.

34 A. T. Stone and J. J. Morgan, *Environ. Sci. Technol.*, 1984, **18**, 450–456.

35 T. S. Natarajan, M. Thomas, K. Natarajan, H. C. Bajaj and R. J. Tayade, *Chem. Eng. J.*, 2011, **169**, 126–134.

36 T. D. Dang, A. N. Banerjee, M. A. Cheney, S. Qian, S. W. Joo and B. K. Min, *Colloids Surf., B*, 2013, **106**, 151–157.

37 C. Yogi, K. Kojima, N. Wada, H. Tokumoto, T. Takai, T. Mizoguchi and H. Tamiaki, *Thin Solid Films*, 2008, **516**, 5881–5884.

38 N. R. de Tacconi, J. Carmona and K. Rajeshwar, *J. Electrochem. Soc.*, 1997, **144**, 2486–2490.

39 A. Mills and J. S. Wang, *J. Photochem. Photobiol., A*, 1999, **127**, 123–134.

40 T. Y. Zhang, T. Oyama, A. Aoshima, H. Hidaka, J. C. Zhao and N. Serpone, *J. Photochem. Photobiol., A*, 2001, **140**, 163–172.